

published as: P. Pasini, C. Chiccoli, C. Zannoni, Liquid crystal lattice models II. Confined systems, in Advances in the Computer Simulations of Liquid Crystals, P. Pasini and C. Zannoni eds., Kluwer, Dordrecht, 121 - 137 (2000)

LIQUID CRYSTAL LATTICE MODELS II. CONFINED SYSTEMS

PAOLO PASINI, CESARE CHICCOLI

*Istituto Nazionale di Fisica Nucleare, Sezione di Bologna
Via Irnerio 46, 40126, Bologna, ITALY*

AND

CLAUDIO ZANNONI

*Dipartimento di Chimica Fisica ed Inorganica, Università di Bologna
Viale Risorgimento 4, 40136, Bologna, ITALY*

Abstract. Monte Carlo simulations of lattice spin models represent a powerful method for the investigation of confined nematic liquid crystals and allow a study of the molecular organization and thermodynamics of these systems. Here some models of confined liquid crystals, such as polymer dispersed liquid crystals, twisted nematic, in-plane switching liquid crystal displays and hybrid aligned films are described together with their computer simulations.

1. Introduction

Confined nematic systems are a class of materials of wide interest both from the technological and basic research point of view [1]. The first aspect is obvious since a large number of electrooptical devices is based on the properties of nematics confined in suitable geometries and boundaries. The academic interest is related to the effects that confinement induces on the phase transitions and on the molecular organization of these systems. This organization in turn stems from a competition between the effects due to surface boundary conditions, to the nematic ordering inside the system and to the disordering caused by temperature. Many experiments and theories have been employed to improve our understanding of these phenomena, but Monte Carlo (MC) simulations seem to be a particularly useful method in

studying relatively small lattices of confined nematics, particularly in the presence of complex geometries or boundary conditions not amenable to analytic solutions. The need of understanding and predicting experiments where orientational ordering plays the key role makes the simple spin models, introduced in the previous Chapter, a convenient and flexible tool to simulate fairly realistic experimental conditions. In particular this technique has proved useful in investigating droplets with fixed surface anchoring [2] mimicking polymer dispersed liquid crystals [3], nematic displays [4, 5] and hybrid aligned nematic cells [6]. Here we wish to present some examples of applications of the model systems.

2. Polymer dispersed liquid crystals

Polymer dispersed liquid crystals (PDLC) [3] are composite materials that consist of microscopic nematic droplets, with typical radii from a few hundred Angström to more than a micron, embedded in a polymer matrix. These systems are interesting for technical applications [3] but PDLC also represent practical realizations of systems exhibiting topological defects of interest in many fields of physics [7]. A number of experimental works have considered different boundary conditions at the droplet surface, for example radial [8, 9], axial [9], toroidal [10] and bipolar [8, 9, 11] that can be obtained by choosing the polymer matrix and the preparation methods. Additional effects of interest come from the application of external, electric or magnetic, fields [8]. MC simulations have been used to study PDLC in a variety of these physical situations: different boundary conditions [12, 14, 16], influence of the anchoring strength at the nematic/polymer interface [13] and the effect of an external applied field [15]. Particular attention has been devoted to simulating quantities that can be directly observed in real experiments in an attempt to bridge the gap with experimental investigations performed on the same systems. For instance, methodologies to calculate powder deuterium NMR lineshapes and textures observable in polarized light experiments corresponding to the microscopic configurations obtained from computer simulations have been developed [2, 15, 16].

The PDLC model used in simulations concentrates on a single droplet and consists of an approximately spherical sample \mathcal{S} carved from a cubic lattice with spins interacting with the Lebwohl-Lasher (LL) potential described in the previous Chapter, while the surface effects are modelled with an external layer of “ghost” spins, \mathcal{G} , with fixed orientations chosen to mimick the desired boundary conditions. The boundary layer acts on the inside particles according to the simple pair interaction:

$$U_{i,j} = -\epsilon_{ij} J \left[\frac{3}{2} (\mathbf{u}_i \cdot \mathbf{u}_j)^2 - \frac{1}{2} \right], \quad \text{for } i \in \mathcal{S}, j \in \mathcal{G}, \quad (1)$$

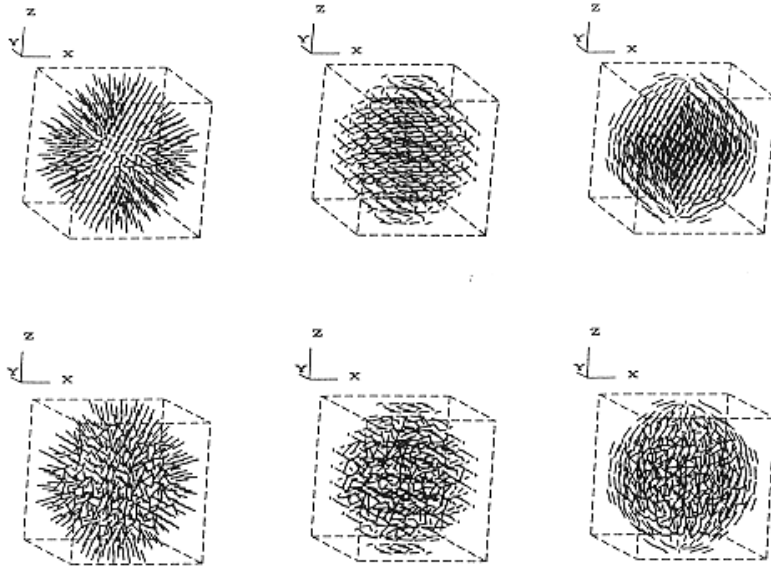


Figure 1. Monte Carlo configurations for a $N = 304$ droplet with radial (left), toroidal (middle) and bipolar (right) surface alignment at a temperature below, $T^* = 0.2$ (top), and one above, $T^* = 1.4$ (bottom) the nematic/isotropic transition are shown [2].

where the sign of the parameter J determines the main direction of anchoring (parallel or perpendicular to the ghost spins) and $|J|$ its strength at the polymer surface. When $J = 1$ the interaction between two neighbors, one on the surface of the nematic droplet and one belonging to the outside matrix, is the same as that between two liquid crystal spins, while $J = 0$ would correspond to a droplet in vacuum. In Figure 1 sample configurations corresponding to the following three different boundary conditions at the interface nematic/polymer are presented:

- i) Radial boundary conditions (RBC), that are imposed by orienting the spins in the matrix normally to the local surface, so that they point towards the center of the droplet.
- ii) Toroidal boundary conditions. (TBC) obtained when the spins in the polymer interface lie in planes perpendicular to the z axis and are oriented tangentially to the droplet surface.
- iii) Bipolar boundary conditions (BBC) for which the ghost spins are oriented tangentially to the droplet surface and belong to planes parallel to the z axis.

In Figure 1 we have included for each case the outer layer of oriented “ghost” spins appropriate to these boundary conditions.

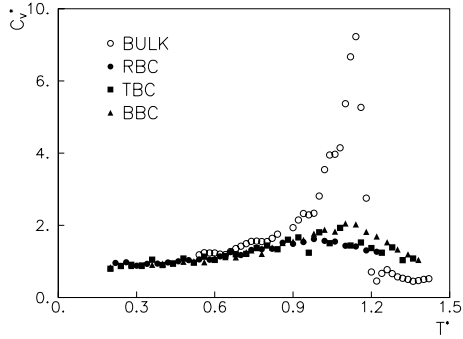


Figure 2. The heat capacity C_V^* versus reduced temperature, T^* , as obtained from Monte Carlo simulations of lattice model droplets with different boundary conditions: radial (RBC), bipolar (BBC) and Toroidal (TBC) and with a bulk simulation. The simulations has been performed on a small lattice ($N = 304$) and with $J = 1$.

From the heat capacity behavior reported in Fig. 2 [2] we see that the nematic-isotropic phase transition is suppressed for small enough confined systems.

To examine the ordering inside the microdroplet various second rank order parameters have been calculated for the systems investigated. The ordinary second rank order parameter, $\langle P_2 \rangle_\lambda$, obtained from diagonalization of the ordering matrix [17] (see previous Chapter), is however not always appropriate as it quantifies the nematic order with respect to an hypothetical global director which may not exist as such. However, MC simulations offer the possibility of evaluating some other order parameters more appropriate to each special case. For example, in case of RBC, it is not possible to distinguish between a perfect ordered radial configuration and a completely disordered system just from the value of $\langle P_2 \rangle_\lambda$ which would vanish in both cases. It is then more useful to define a radial order parameter, $\langle P_2 \rangle_R$ [12]:

$$\langle P_2 \rangle_R = \frac{1}{N} \sum_{i=1}^N P_2(\mathbf{u}_i \cdot \mathbf{r}_i), \quad (2)$$

where \mathbf{r}_i is the radial vector of the i th spin. For a perfect hedgehog configuration $\langle P_2 \rangle_R = 1$, while for a truly disordered system $\langle P_2 \rangle_R = 0$. Following the same reasoning it is possible to define a configurational order parameter, $\langle P_2 \rangle_C$, which tends to one for a configuration perfectly ordered according to the idealized structure induced by the boundary conditions used. Thus

$$\langle P_2 \rangle_C = \frac{1}{N} \sum_{i=1}^N P_2(\mathbf{u}_i \cdot \mathbf{c}_i), \quad (3)$$

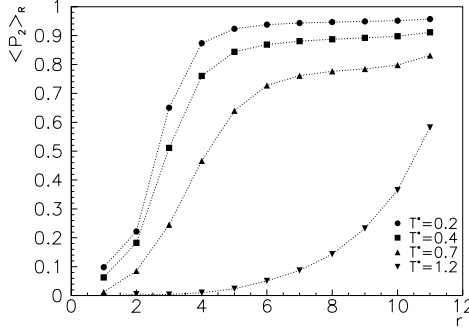


Figure 3. The radial order parameter, $\langle P_2 \rangle_R$, versus distance r starting from the center of the droplet. The results are obtained from Monte Carlo simulations of a RBC lattice model droplet with 5832 spins at some selected temperatures.

where \mathbf{c}_i is the direction corresponding to the local surface induced alignment. For example in the bipolar case \mathbf{c}_i is a local meridian that lies on the plane defined by the droplet axis (z axis) and the radial vector \mathbf{r}_i of the particle while being perpendicular to \mathbf{r}_i itself.

An investigation of these configurational order parameters across the sample is interesting to test theories of the molecular organisation inside the droplet. In MC this can be achieved dividing the droplet in concentric shells and calculating the relevant quantities in each region so as to have the variation of the ordering going from the center to the border of the system. As an example, the behavior of $\langle P_2 \rangle_R$ with respect to the distance from the center is reported in Fig. 3 at some selected temperatures. These results show, in the nematic region, a ordered core at the center of the droplet, consistent with a ring disclination [18, 19], with a radius which becomes larger as the temperature increases.

The standard nematic order parameter $\langle P_2 \rangle_\lambda$ shows, quite reasonably, an opposite behavior; i.e. it is a maximum at the center of the droplet where the aligned core is found and decreases approaching the surface where the spins are radially oriented. In Figure 4 the order parameters $\langle P_2 \rangle_\lambda$, for the three different boundary conditions here considered, are shown as a function of the distance from the droplet center in lattice units. In the right hand side plates of Fig. 4 $\langle P_2 \rangle_\lambda$ is plotted against a scaled distance r/r_{max} , where r_{max} is the radius of the sphere, to investigate if the ordering inside the droplet depends on the system size or if the behavior is just the same in these reduced units. As mentioned earlier we expect, for the radial case, the nematic order to be greater near the core of the droplet (inner shell) and to decrease in the other shells. It is interesting to notice that in the RBC case the size of the aligned core does not depend on the droplet size and has a radius of about 3-4 lattice units [19] (see Figure 4 top) for all the

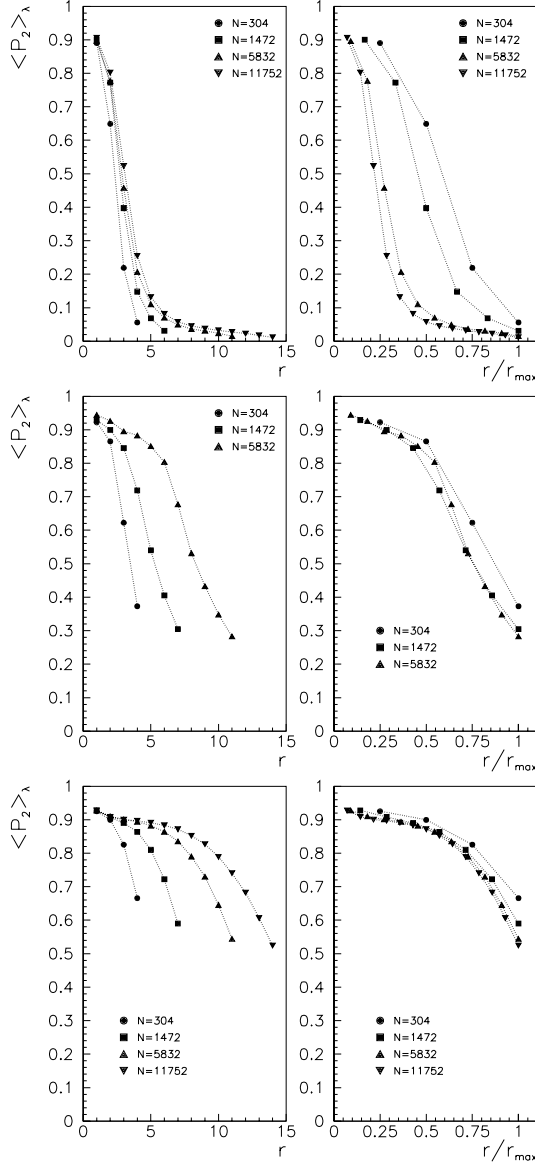


Figure 4. The nematic order parameter, $\langle P_2 \rangle_\lambda$, versus distance r starting from the center of the droplet. The results are obtained from Monte Carlo simulations of various sizes with radial (top), toroidal (middle) and bipolar (bottom) boundary conditions. The right plates show the curves plotted against a normalized distance r/r_{max} .

system sizes studied. This hints that the core size is a true material property [19] rather than being dependent on the droplet size. The picture changes completely when going to a planar surface anchoring: the nematic ordering

at the surface becomes larger for the toroidal boundary conditions and then even larger for the bipolar case with respect to the radial one (Fig.4 *middle* and *bottom*). Moreover the aligned region at the center becomes larger and, above all, its size increases linearly with the droplet radius yielding almost superimposed curves for the different system sizes, as shown on the right in Fig. 4 *middle* and *bottom*). We can then say that the behavior of the planar (toroidal and bipolar) boundary condition systems is the same in scaled units, differently from that of RBC.

The similarity in the behavior of properties calculated for different sample sizes strengthens the argument that each of our spins could really be considered to represent a microdomain of some tens of particles, and that our results also are applicable to droplets in the micron size, that have been investigated experimentally [9] by optical techniques.

A particularly interesting case comes from the application of an external field, a situation that corresponds to many real experiments. At the microscopic level this is modeled by adding an extra term to the hamiltonian of the system (1). Assuming second rank interactions ($L = 2$) the total configuration energy is written as:

$$U = - \sum_i^N \left\{ \sum_j^N \epsilon_{ij} P_2(\mathbf{u}_i \cdot \mathbf{u}_j) + \epsilon \xi P_2(\mathbf{u}_i \cdot \mathbf{B}) \right\} \quad , j > i, \quad (4)$$

where \mathbf{B} is a unit vector along the field direction and the parameter ξ depends on the anisotropy of the electric or magnetic susceptibility and on the field intensity. In this case too we have defined an appropriate second rank order parameter, which now expresses the molecular alignment with respect to the field, $\langle P_2 \rangle_B$:

$$\langle P_2 \rangle_B = \frac{1}{N} \sum_{i=1}^N P_2(\mathbf{u}_i \cdot \mathbf{B}). \quad (5)$$

Examples of these thermodynamic observables have been presented for various physical situations for the three boundary conditions listed above in our works on PDLC systems [15, 16].

2.1. MOLECULAR ORGANIZATION AND DEUTERIUM NMR SPECTRA

Monte Carlo simulations allow us to generate, apart from averages of thermodynamic observables, full sets of coordinates and angles representing instantaneous configurations of the lattice that can be used for visualization (cf. Fig. 1) or to calculate other quantities of interest such as, for example, polydomain deuterium NMR lineshapes for the model system of fictitious molecules.

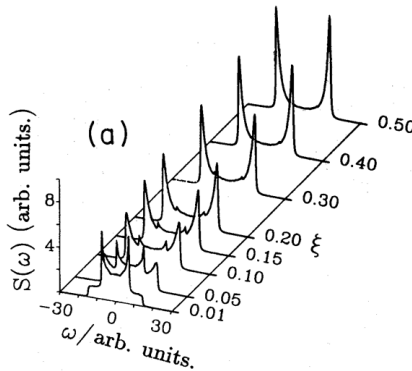


Figure 5. An example of NMR lineshapes as obtained from Monte Carlo simulations of a model droplet with radial boundary conditions at a reduced temperature $T^* = 0.4$. The applied external field is directed along the z axis and its intensity is modulated by the parameter ξ [15].

Deuterium NMR of deuterated liquid crystals has been frequently used in studying PDLC droplets [9], particularly when the droplets are so small that standard optical methods are not viable. The use of ^2H NMR allows focusing on the molecules inside the droplet (the only deuterated ones) thus giving in principle a direct handle on their properties. Each deuteron with quadrupole coupling constant ν_Q and angle θ between effective quadrupole axis and molecular axis provides a couple of lines at frequency

$$\omega_Q(\cos \beta_i) = \pm \frac{3}{4} \nu_Q P_2(\cos \beta_i) P_2(\cos \theta), \quad (6)$$

where β_i is the angle between molecule and field axis, and uniaxial symmetry of the tensor and of the molecule are assumed. If the effect of the NMR spectrometer magnetic field on the configuration is negligible, as it is the case at least for sub-micron droplets [20] then field effects due to the applied external field can be examined.

In order to calculate simulated lineshapes from the Monte Carlo configurations we have assumed a system of fictitious deuterated molecules with axis of effective molecular uniaxial symmetry corresponding to that of the spins [15] as obtained for our configurations. Moreover, if molecular diffusion can be assumed to be negligible at the chosen experimental conditions, then the deuterium NMR spectrum becomes a powder like one and can give information on the director distribution or more generally on the molecular organization. These apparently rather stringent conditions have been shown to hold in various experimental studies [8, 11].

In practice the total spectrum for a configuration is calculated as the sample average

$$\mathcal{S}(\omega) = \left\langle \mathcal{S}[\omega, \omega_Q(\cos \beta_i), T_2^{-1}] \right\rangle_S \quad (7)$$

$$= \frac{1}{N} \sum_{i=1}^N \mathcal{S}[\omega, \omega_Q(\cos \beta_i), T_2^{-1}] \quad (8)$$

where N is the number of molecules in the droplet. Every particle provides a line shape contribution.

$$\mathcal{S}[\omega, \omega_Q(\cos \beta_i), T_2^{-1}] = \sum_{p=\pm 1} \frac{T_2^{-1}}{[\omega - p\omega_Q(\cos \beta_i)]^2 + [T_2^{-1}]^2}. \quad (9)$$

In Ref. [15] we have used data appropriate to *4'-methoxy-4-cyanobiphenyl-d₃* (10CB): $\nu_Q = 175\text{Hz}$ and $\theta = 59.45$ degrees corresponding to the angle between CD_3 axis and molecular axis and consistent with the assumption of fast rotation of the CD_3 group, as from Ref. [8] and an intrinsic line width $T_2^{-1} = 200\text{Hz}$. This establishes a correspondence between kHz and the arbitrary units used for the frequency scale. The resulting spectrum is then further averaged over a number of configurations to improve the signal to noise ratio. An example of NMR line shapes calculated from an average over droplet configurations of a RBC droplet with $N=5832$ at different field strengths, ξ , is shown in Fig. 5 [15]. The deuterium splitting is a maximum when the molecules have their principal axis parallel to the applied field. At the lowest field, the droplet configurations is characterized by a near perfect hedgehog configuration and this gives rise to a lineshape characteristics of an essentially three dimensionally isotropic distribution of molecules with respect to the direction of the applied field. At stronger fields the population of molecules parallel to the field increases and the lineshape progressively reduces to a doublet corresponding to the parallel splitting.

In the case of RBC droplets the simulation results are compatible with a first order transition in the microscopic organization inside the droplet as the strength of the applied field increases as predicted by Dubois-Violette and Parodi [21] for a similar system.

2.2. POLARIZED LIGHT TEXTURES

Another experimental technique used to investigate micrometer size droplets is polarized light microscopy [9]. Also this kind of experimental observables can be calculated starting from the Monte Carlo configurations of the lattice spin model [16] exploiting a standard matrix approach which has been

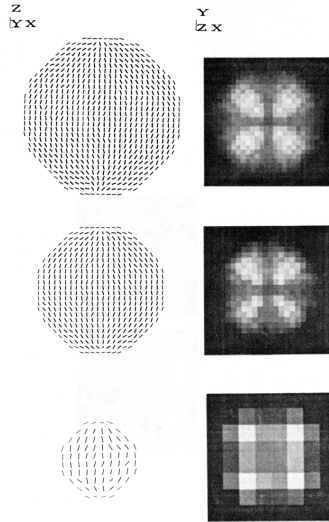


Figure 6. An example of snapshots and polarised optical images as obtained from Monte Carlo simulations of model droplets with bipolar boundary conditions. Three different sizes with 11752 (top), 5832 (middle) and 304 (bottom) spins at a reduced temperature $T^* = 0.4$ are shown.

employed in calculations based on continuum theory [9, 22, 23]. The basic idea in the matrix approach is that ray optics can be used and that each site in the droplet is described by a Müller matrix [24]. Then the light ray passing through a row of particles across the droplet is retarded by the matrix resulting from the product of the Müller matrices corresponding to each site in the light path. Each matrix involves the angles ϕ_j and θ_j , describing the orientation of a domain j , taken from the simulation data, and the phase difference which depends on the thickness of the layer, h , the wave length, λ , and the refractive indices, n_0 and n_e . In Ref. [16] we have used $h = 5.3\mu m/(2r_{max})$ (r_{max} is the radius of the droplet in lattice units), $\lambda = 545nm$, $n_0 = 1.5$ and $n_e = 1.7$, similar to those of the nematic liquid crystal 5CB [9]. Since we assume the local domain to be basically unchanged throughout the simulations, thus only describing the disordering of each domain with respect to the others, we have arbitrarily taken this intrinsic refractivity to be constant with temperature.

To observe the light retarded by the droplet we assume to have crossed polarizers placed at each side of the sample cell, \mathbf{P}_{in} and \mathbf{P}_{out} , and the resulting Stokes vector of the polarized and retarded light beam is thus

given by [22, 23]:

$$\mathbf{s} = \mathbf{P}_{out} \prod_j \mathbf{M}_j \mathbf{P}_{in} \mathbf{s}_{in}, \quad (10)$$

where \mathbf{s}_{in} corresponds to the Stokes vector of unpolarized light. The intensity is proportional to the first element in the output Stokes vector \mathbf{s} . To improve the quality of the optical image we further average over a number (typically around 20) equilibrated configurations. A texture obtained from configurations defined by a lattice of $22 \times 22 \times 22$, corresponding to a droplet of 5832 particles, provides a projection of 22×22 pixels perpendicular to the direction of the retarded and polarized lightbeams. The intensity of each pixel is grey coded for each picture with a normalized scale going from black, lowest intensity of light, to white, highest intensity, with 32 different grey levels. As an example the simulated optical patterns as obtained from Monte Carlo simulations of BBC droplets of different sizes are shown in Fig. 6. It is clear from these images that the basic features of the optical textures, as obtained experimentally by Doane group [9], are reproduced even with the smallest droplet size with only 304 spins.

3. Liquid crystal displays

Other quite different types of confined systems are the one dimensional ones, where a thin nematic film is confined between two surfaces as in the cells employed in Liquid Crystal Displays (LCD). Although these devices have been popular for two decades a large part of the know-how on them seems to be empirical or based on macroscopical continuum models. However, the range and scale of computer modelling have now grown to the point where it is possible to try and attempt a complete simulation of a model display starting from microscopic interactions. The techniques described in the previous section allow to simulate LCD images while at the same time MC can provide a unique tool for understanding and predicting ordering and microscopic organization inside the display cell. We briefly describe here the lattice simulations of two types of LCD: the Twisted Nematic (TN) [25] and a more recently proposed one based on the In-Plane Switching effect [26].

3.1. TWISTED NEMATIC DISPLAY

The spin model we employ tries to catch the essential features of the well known TN cell. The fixed “ghosts” on the top of the cell are oriented perpendicularly to those on the bottom while both are parallel to the cell surfaces (cf. Fig. 7 *left*). The alignment induced by these surfaces tends to propagate inside the liquid crystal cell producing a twisted nematic con-

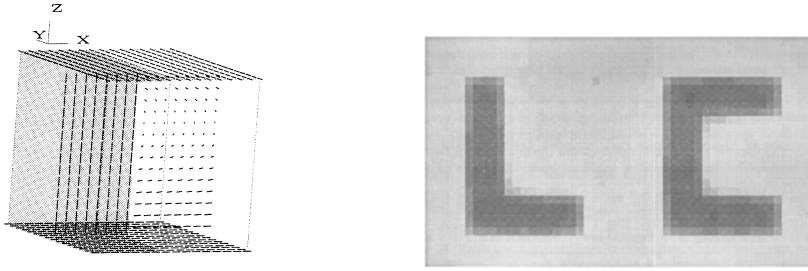


Figure 7. The twisted nematic lattice model. (Left): The simulation cell with the ordered surfaces and the regions in presence (grey) and absence of an applied field. (Right:) An example of a simulated optical image.

figuration. Periodic boundary conditions are employed around the other four faces of the cell. Moreover the lattice is divided in a regular array of sublattices where a field can be applied or not. At a microscopic level this is realized adding a local second rank term to the LL hamiltonian as in Equation (4). The field \mathbf{B} is directed along the z-axis of the display, i.e. perpendicular to the oriented surfaces, and a factor $F = 1$ or 0 in front of the second term in Equation (4) acts as a switch to turn on or off the local external field. We assume that an electric field is applied and we take $\xi > 0$, corresponding to a material with positive dielectric anisotropy. When a sufficiently strong field is applied (*on* region), the molecules on which it acts align on average along the field direction, while the helical structure is conserved in the rest of the cell (*off* region), as schematically shown in Figure 7 (*left plate*). An helical order parameter appropriate to determin-

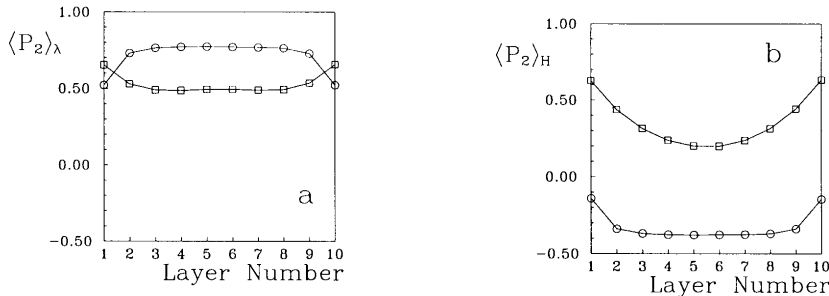


Figure 8. The standard nematic order parameter $\langle P_2 \rangle_\lambda$ (left) and helical order parameter $\langle P_2 \rangle_H$ (right) in regions with (squares) and without (circles) the applied field are illustrated for each layer of the display. The simulation was made at a scaled temperature, $T^* = 1.0$, and with the applied field strength, $\xi = 1.0$.

ing the order in the different layers and in the two regions: with external

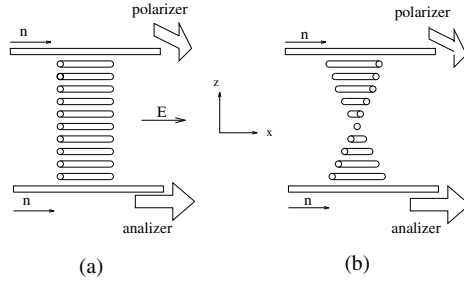


Figure 9. A sketch of the operation mode of the In-Plane Switching LC display with the light propagation direction along the z axis. The alignment direction of the surfaces is indicated by \mathbf{n} . (a) Field off: the polarized light is not transmitted through the cell; (b) Field on: a layer of nematic molecules rotates and the director twist changes the polarization of the incoming light which now passes through the analyzer.

field *off* or *on* can be introduced. This more specific microscopic quantity expressing the deviation from the ideal twist configuration, is the *helical order parameter*, $\langle P_2 \rangle_H$ defined [4] as follows:

$$\langle P_2 \rangle_H = \frac{1}{N_L} \sum_{i=1}^{N_L} P_2(\mathbf{u}_i \cdot \mathbf{t}_i), \quad (11)$$

where N_L is the number of particles contained in the L th layer and \mathbf{t}_i is the ideal twist direction at point i . In the limiting case that all the particles lie in the direction defined by the discretized helix between the bottom and top surfaces $\langle P_2 \rangle_H = 1$. In the field *on* regions $\langle P_2 \rangle_H$ becomes negative corresponding to the molecules being on average perpendicular to the ideal helix axis. In Fig. 8 the $\langle P_2 \rangle_\lambda$ and $\langle P_2 \rangle_H$, in the regions with and without the applied field, are shown. $\langle P_2 \rangle_\lambda$ is, except near the surface, higher in the *on* than in the *off* regions.

The link between simulation and experiment can be made more direct calculating the appearance of the display (Figure 7, right). For the perfectly twisted organization we obtain the largest intensity of transmitted light, and the *off* regions become light grey while the *on* regions, corresponding to written symbols, are darker, or ideally black. The appearance of display hints that simulations could start to be employed in modeling complex liquid crystal devices.

3.2. IN-PLANE SWITCHING EFFECT DISPLAY

In this device the top and bottom transparent cell surfaces are treated to induce homogeneous, i.e. surface parallel, alignment along the same direction (x in Fig. 9). A polarizer and an analyzer, with orthogonal polarization directions (for example along the x and y axis) are placed respectively above and below the cell. Thus a display element, a pixel say, does not let light through with no field applied and is black. Differently from the twisted nematic case, the liquid crystalline material filling the cell is chosen to have a negative dielectric anisotropy. The lateral switching effect is due to the application of an external electric field (see Fig. 9) across two electrodes placed at a certain distance from the surfaces and in a plane orthogonal to the light direction. The field is applied across the cell, and ideally it acts only on the molecules belonging to a thin intermediate layer of the liquid crystal sample. Notice that the direction of the applied field is parallel to the surface alignment direction but, due to the negative dielectric anisotropy, the molecules subjected to the field tend to rotate by 90 degrees so that a twisted alignment is induced between this intermediate layer and the two aligned surfaces.

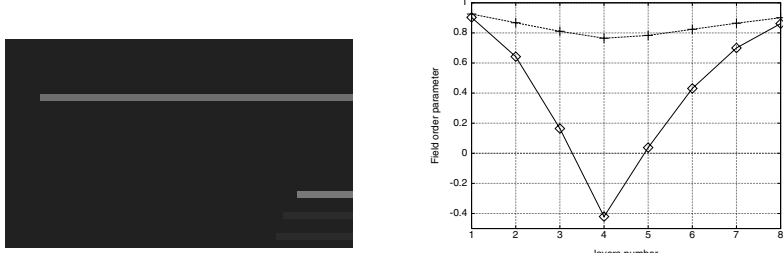


Figure 10. (Left:) An example of simulated optical image of a in-plane switching display as obtained by a lattice spin model simulation. (Right:) The order parameter with respect to the field direction (cf. Eq. 5) calculated for the same sample in the region where the field is active (diamonds) or off (plus).

Contrary to the usual twisted nematic display the light is thus transmitted only where the effect of the field is sufficiently strong and the background of the image is black. A simulated in-plane liquid crystal display image is shown in Fig. 10 together with the field order parameters calculated at each layer of the cell.

4. Hybrid aligned nematic film

The third type of confined system we consider here is a model of an hybrid cell, with random planar orientation on the bottom surface and

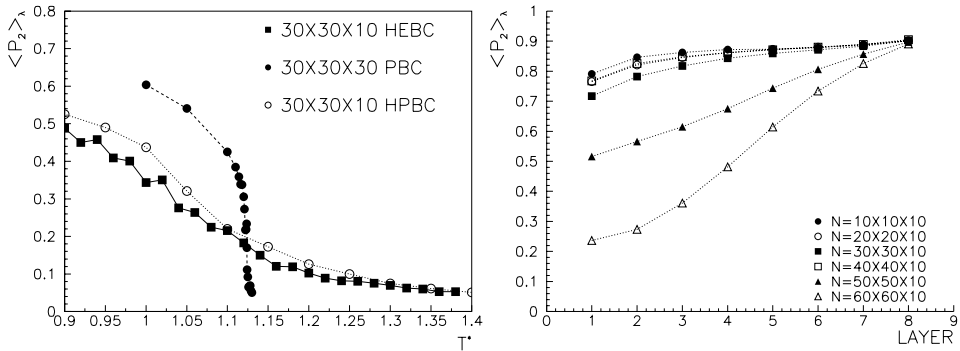


Figure 11. (Left): The order parameter dependence on temperature in an HAN system with empty (HEBC) or periodic (HPBC) lateral boundary conditions. As a comparison the bulk behavior is also reported. (Right): The order parameter calculated at each layer of the cell for different lateral size systems.

homeotropic, normal orientation at the top. These conditions have been experimentally realized [6] e.g. placing a liquid crystal film on top of an isotropic liquid substrate such as polyethyleneglycol or glycerine and leaving a free air/liquid crystal surface. The interest on these systems is related to one of the most important and telling properties of liquid crystals: the structure of their topological defects, that is points or lines along which it is impossible to define an order parameter, under different conditions [7]. Lavrentovich [6] has demonstrated that this hybrid nematic liquid crystal films produce very interesting polarized-microscopy textures that are probably due to the presence of the two competing boundary conditions. Also in this case the MC method proves quite useful in studying these patterns and allows a precise control over the factors involved, such as thickness and anchoring strength.

The hybrid aligned nematic (HAN) cell [27] is mimicked assuming a $L \times L \times h$ lattice with suitable boundary conditions [28]. The spins of the bottom layer, $z = 0$, have random fixed orientations in the horizontal (x, y) plane, while those of the top layer, $z = h$, are fixed along the surface normal. Open, i.e. empty space, boundary conditions are assumed on the four planes surrounding the cell instead of the usually employed periodic BC with identical replicas surrounding the sample [28]. This artificial periodicity causes no fundamental artefacts in the modelling of uniform states.

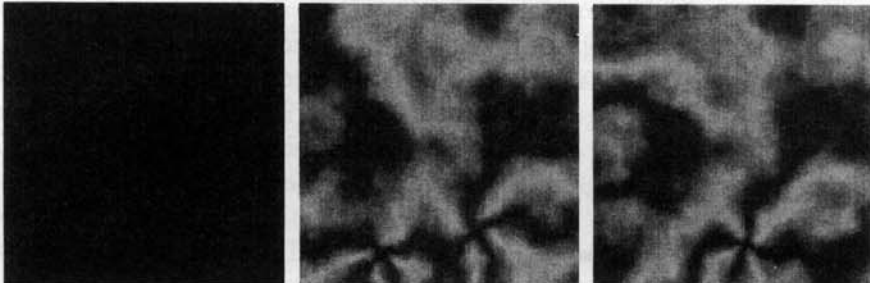


Figure 12. The appearance of a stable point defect in an hybrid nematic film as obtained by MC simulations of a $100 \times 100 \times 12$ lattice system [28]. The images correspond to 100, 6000 and 80000 MC evolution cycles from left to right respectively.

However, when the ground state contains topological defects, they might be incompatible with periodic BC and hence our reason for not using them. The molecular organization resulting from this conflicting surface boundaries is then inhomogeneous across the sample going from the disordered configuration of the first layer to the aligned one of the last layer. The system goes from an ordered to an isotropic phase at a temperature which is approximately from 5 to 10% lower than that exhibited by the LL model [29], as we see in Fig 11 (*left*). Moreover there are no evident changes in the phase transition behavior increasing the horizontal dimensions of the cell. The defects do not appear until the lateral size L becomes much larger than h (e.g. $L \geq 50$ for $h = 10$). For films with small and large L/h , the director is strongly deformed in the vertical plane, obviously following the antagonistic boundary conditions at $z = 0$ and $z = h$. The horizontal director field is uniform, although not perfectly, and only small variations of the director exist. The situation dramatically changes for large L/h where there are strong and stable horizontal deformations associated with topological defects. The texture develops from black to a set of brushes, with each defect marked by four brushes emerging from its core [30]. The defects are of strength $m = \pm 1$, i.e., the director field undergoes a $\pm 2\pi$ rotation as one goes once around the defect core. The absolute value $|m| = 1$ is the lowest possible topological charge of a defect in a HAN film. The texture evolves as the system anneals, but the defects do not disappear even in the

longest runs performed (120000 cycles, where a cycle is a full lattice update) even though they occasionally migrate outside the sample. The core of the defect is located near the lower surface; the distortions vanish as one moves towards the upper plate and the molecules reorient along the z axis. Note that the results described above are specifically related to the hybrid alignment of the film. In this case the nematic order parameter $\langle P_2 \rangle_\lambda$ (see, e.g. [17]) across the film changes substantially for the larger lattices but not for the small ones (see Fig. 11, right plate).

A striking result of the MC simulations is that the model based exclusively on pure nearest-neighbors molecular interactions mimics the long-range deformations with topologically stable defects in agreement with continuum theory predictions.

5. Conclusions

We have described lattice spin models for the simulation of various confined nematic systems. The biggest advantage of Monte Carlo simulations is the possibility of investigating the system at a microscopic level. Moreover, apart from the usual thermodynamic properties it is possible to define and calculate specific configurational order parameters suitable for the different types of systems under investigation. Molecular organizations can be visualized as snapshots but the optics of a simulated device can also be calculated as shown for applications to models of nematic liquid crystal displays (LCD), polymer dispersed liquid crystals (PDLC), and hybrid aligned films.

Acknowledgments

We thank University of Bologna, MURST, CNR and INFN (grant I.S. BO12) for support and our collaborators and students for their invaluable help.

References

1. Crawford, G.P. and Žumer, S. (eds.) (1995) *Liquid Crystals in Complex Geometries Formed by Polymer and Porous Networks*, Taylor and Francis, London.
2. Chiccoli, C., Pasini, P., Semeria, F., Berggren, E. and Zannoni, C. (1995) *Mol. Cryst. Liq. Cryst.* **266**, 241 and references therein.
3. Crawford, G.P. and Doane, J.W. (1992) *Condens. Matter News*, **1**, 5.
4. Berggren, E., Zannoni, C., Chiccoli, C., Pasini, P. and Semeria, F. (1995) *Int. J. Mod. Phys. C*, **6**, 135.
5. Chiccoli, C., Guzzetti, S., Pasini, P. and Zannoni, C. (1998) *Int. J. Mod. Phys. C*, **9**, 409.
6. Lavrentovich, O.D. (1992) *Liq. Cryst. Today*, **2**, 3 and references therein.
7. Mermin, N.D (1976) *Rev. Mod. Phys.*, **51**, 591.
8. Golemme, A., Žumer, S., Doane, J.W. and Neubert, M.E. (1988) *Phys. Rev. A*, **37**, 559.

9. Ondris-Crawford, R., Boyko, E.P., Erdmann, B.G., Žumer S. and Doane, J.W. (1991) *J. Appl. Phys.*, **69**, 6380.
10. Drzaic, P. (1988) *Mol. Cryst. Liq. Cryst.*, **154**, 289.
11. Aloe, R., Chidichimo, G. and Golemme, A. (1991) *Mol. Cryst. Liq. Cryst.*, **203**, 1155.
12. Chiccoli, C., Pasini, P., Semeria F. and Zannoni, C. (1990) *Phys. Lett.*, **150A**, 311.
13. Chiccoli, C., Pasini, P., Semeria F. and Zannoni, C. (1992) *Mol. Cryst. Liq. Cryst.*, **212**, 197.
14. Chiccoli, C., Pasini, P., Semeria F. and Zannoni, C. (1992) *Mol. Cryst. Liq. Cryst.*, **221**, 19.
15. (a) Berggren, E., Zannoni, C., Chiccoli, C., Pasini, P. and Semeria, F. (1992) *Chem. Phys. Lett.*, **197**, 224. (b) (1994) *Phys. Rev. E*, **49**, 614.
16. Berggren, E., Zannoni, C., Chiccoli, C., Pasini, P. and Semeria, F. (1994) *Phys. Rev. E*, **50**, 2929.
17. Zannoni, C. (1999) Chapter 2 of this volume.
18. Schopol N. and T.J. Sluckin (1988) *J. Phys. France*, **49**, 1097.
19. Chiccoli, C., Pasini, P., Semeria, F., Sluckin, T.J. and Zannoni, C. (1995) *J. de Physique II*, **5**, 427.
20. Crawford, G.P., Ondris-Crawford, R., Žumer, S. and Doane, J.W. (1993) *Phys. Rev. Lett.*, **70**, 1838 .
21. Dubois-Violette, E. and Parodi, O. (1969) *J. de Physique*, Colloq. **30**, C4-57.
22. Xu, F. , Kitzrow, H.-S. and Crooker, P.P. (1992) *Phys. Rev. A*, **46**, 6535.
23. Kilian, A. (1993) *Liq. Cryst.*, **14**, 1189.
24. Schellman, J.A. (1988) in *Polarized Spectroscopy of Ordered Systems*, Samori', B. and Thulstrup, E.W.(eds.), Kluwer, Dordrecht, p. 231.
25. Schadt, M. (1989) *Liq. Cryst.*, **5**, 57.
26. Baur, G. Kiefer, R., Klausmann, H. and Windscheid, F. (1995) *Liquid Crystals Today*, **5**, 13 and References therein.
27. O.D. Lavrentovich and V.M. Pergamenshchik, (1995) *Int. J. Mod. Phys. B*, **9**, 2839.
28. Chiccoli, C. O.D. Lavrentovich, Pasini, P. and Zannoni C. (1997) *Phys. Rev. Lett.*, **79**, 4401.
29. Chiccoli, C., Pasini, P. and Zannoni, C. (1999) *Mol. Cryst. Liq. Cryst.* (in press).
30. Kleman, M (1983) *Points, Lines and Walls* Wiley, New York.
31. Fabbri, U. and Zannoni, C. (1986) *Mol. Phys.*, **58**, 763.

Table of Contents

6 LIQUID CRYSTAL LATTICE MODELS II.	
 CONFINED SYSTEMS	121
1 Introduction	121
2 Polymer dispersed liquid crystals	122
2.1 Molecular organization and deuterium NMR spectra	127
2.2 Polarized light textures	129
3 Liquid crystal displays	131
3.1 Twisted nematic display	131
3.2 In-plane Switching Effect Display	133
4 Hybrid aligned nematic film	134
5 Conclusions	137